Energetic stability, equilibrium geometry, and the electronic properties of Ca/Si(111) surfaces

R. H. Miwa
Faculdade de Física, Universidade Federal de Uberlândia, Caixa Postal 593, 38400-902 Uberlândia, MG, Brazil
(Received 11 February 2005; revised manuscript received 4 May 2005; published 11 August 2005)

We have performed an *ab initio* theoretical investigation of the energetic stability, equilibrium atomic geometry, and scanning tunneling microscope (STM) images of the Ca/Si(111) surface. We have considered the (3×1), (3×2), and (2×1) structural models for Ca coverage of 1/3 ML, 1/6 ML, and 1/2 ML, respectively. Our total energy results indicate that the (3×1) phase is not expected to occur, even for Ca-rich conditions. In the (3×2) phase the Ca adatoms lie on the *T*4 sites along the surface trench separated by Si honeycomb chains. Similarly, in the (2×1) phase the Ca adatoms are adsorbed on the *T*4 sites of the surface trench separated by Si zigzag chains. The equilibrium geometries and electronic charge transfers between Ca adatoms and Si(111) surface for the (3×2) and (2×1) phases have been detailed. Our simulated STM images indicate that the higher-lying occupied states are located on the topmost Si atoms along the chains, while the empty states lie on the Ca adatoms, forming bright spots and stripes on the (3×2) and (2×1) surfaces. For occupied states, the simulated STM images confirm the experimentally verified $2\times$ modulation along the honeycomb chains in the Ca/Si(111)-(3×2) surface, induced by attractive interactions between Ca adatoms and the nearest-neighbor Si atoms. Finally we have calculated the electronic band structures for the energetically stable (3×2) and (2×1) phases of the Ca/Si(111) surface, and compared (in detail) with the recent experimental findings.

DOI: 10.1103/PhysRevB.72.085325 PACS number(s): 68.43.Hn, 73.20.At

I. INTRODUCTION

One-dimensional (1D) systems obtained through metal deposition on semiconductor surfaces exhibit a number of new and exotic electronic and structural properties compared with the ones in the 3D bulk phase. For instance, Peierls-like instability[1] and anisotropic behavior of image states[2] have been verified along the In wires on the In/Si(111)-(4×1) surface. Similarly, under certain growth conditions, well ordered self-organized Bi lines with more than 500 nm free of defects (kinks or vacancies) have been observed on the Si(001) substrate.[3–7] In parallel with this, *ab initio* theoretical investigations have been done in order to clarify the structural and energetic properties of these 1D systems.[8–11] In general, due to its technological appeal, the silicon substrate has been employed for the majority of 1D-metal/semiconductor systems.

Recently, self-assembled 1D systems obtained by deposition of alkali metals (AM's) or alkali-earth metals (AEM's) on Si(111) have attracted several experimental works. For a coverage of 1/3 monolayer (ML), AM/Si(111) surfaces exhibit a (3×1) reconstruction with the AM adatoms adsorbed along the surface trench between the Si honeycomb chains.[12] These structures are semiconducting, as expected based on electron counting analysis since we have an even number of valence electrons in the 3×1 surface unit cell. However, the same good agreement between observed electronic structure and surface reconstruction has not been verified for AEM's adsorbed on Si(111). Indeed, for Mg on Si(111), photoemission experiments performed by An *et al.*[13] indicated a semiconducting character for the Mg/Si(111)-(3×1) surface. This surface has an odd number of valence electrons per 3×1 unit cell and thus should be metallic within the electron counting analysis. Further low-energy electron diffraction (LEED) images, obtained by Kubo *et al.*,[14] confirmed the Mg/Si(111)-(3×1) phase for a Mg (Si) coverage of 1/3 ML (4/3 ML). However, in the same experimental study, scanning tunneling microscopy (STM) results indicated a local (3×2) atomic ordering on the Mg/Si(111) surface. They verified bright protrusions on the Mg adatoms, for empty-state STM images, and suggested that the (3×2) ordering was "caused by a Mg-Mg interaction" parallel to the honeycomb chains. In subsequent (STM) experimental works, Saranin *et al.*[15,16] extended such AEM-AEM atomic interactions to explain the observed (3×2) ordering on the Ca/Si(111) surface.

The Ca/Si(111) surface was initially investigated by core-level and angle-resolved photoemission experiments,[17] where the authors observed a (3×1) reconstruction for a Ca concentration of 1/3 ML. However, similar to the Mg/Si(111)-(3×1) surface, the Ca/Si(111)-(3×1) surface exhibits a semiconducting character, which is also in disagreement with the electron counting analysis. Further investigations, including STM images and *ab initio* total energy calculations, confirmed the (3×1) phase and the semiconducting character for the Ca/Si(111) surface with Ca coverage of 1/3 ML.[18] For a Ca coverage of 1/2 ML, the Ca/Si(111) surface exhibits a semiconducting (2×1) phase. In this case, the semiconducting character of the (2×1) phase is in accordance with the electron counting arguments, while a Peierls-like instability was proposed in order to explain the unexpected electronic behavior along the Ca lines for the (3×1) phase.[18] Further STM studies[19] supported the (3×2) phase proposed in Refs. 15 and 16. They find a $2\times$ modulation parallel to the Ca lines, giving rise to the (3×2) phase, however keeping the Ca coverage of 1/3 ML.

Very recently, Sakamoto *et al.*[20] performed a detailed structural investigation of Ca/Si(111) surfaces by using

core-level photoemission experiments. Instead of (3×1) or (3×2) phases with a Ca coverage of 1/3 ML, they proposed a (3×2) phase with a Ca coverage of 1/6 ML, with the Ca adatoms adsorbed along the surface trench. In this case we have an even number of valence electrons per 3×2 unit cell, thus explaining the semiconducting character of the Ca/Si(111)-(3×2) surface by the simple electron counting model. It is worth pointing out that the (3×2) phase with an AEM coverage of 1/6 ML was already proposed for the Ba/Si(111)-(3×2) surface.[21] In addition, recent angle-resolved photoelectron spectroscopy (ARPES) experiments[22,23] not only confirmed the semiconducting character of the Ca/Si(111) surface, but also supported the (3×2) and (2×1) phases for Ca coverages of 1/6 ML and 1/2 ML, respectively. Those experimental works provided a fundamental understanding of the electronic and structural properties of AEM's on Si substrates. However, as pointed out in Ref. 23, there is no theoretical investigation focusing the energetic stability, equilibrium atomic geometry, and electronic properties of the Ca/Si(111)-(3×2) and -(2×1) surfaces.

In this paper we present a detailed *ab initio* theoretical investigation of Ca-induced Si(111)-(3×2), -(3×1), and -(2×1) surfaces. Comparing the total energies of the (3×2) and (3×1) phases, with Ca coverages of 1/6 and 1/3 ML, respectively, we find that the (3×1) phase is not expected to occur. The equilibrium geometries of the (3×2) and (2×1) phases were compared with the experimental findings. In addition, based on surface charge transfer analysis, we inferred a qualitative picture for the core-level photoemission results presented in Ref. 20. Our simulated STM images compare very well with the experimental findings, where we observe the $2\times$ modulation (occupied states) and bright protrusions (empty states) along the honeycomb chains for the (3×2) phase. Finally, we detailed the electronic band structure of the energetically stable Ca/Si(111)-(3×2) and -(2×1) surfaces and compared with the experimentally obtained ARPES results.

II. THEORETICAL APPROACH

The *ab initio* total energy calculations were performed in the framework of the density functional theory.[24] We have used the SIESTA code,[25] which performs fully self-consistent calculations solving the Kohn-Sham (KS) equations.[26] The KS orbitals are expanded using linear combinations of pseudoatomics orbitals.[27] We have used a double-ζ basis with polarization functions.[28] The calculations were done with the local density approximation, using the Ceperley-Alder correlation[29] as parametrized by Perdew and Zunger.[30] The electron-ion interaction was treated by using norm-conserving, *ab initio*, fully separable pseudopotentials.[31] A cutoff of 200 Ry for the grid integration was utilized to represent the charge density. The Ca/Si(111) surfaces were simulated by using the slab method, with 10 ML of Si plus a vaccum region of 10 Å. The Si dangling bonds of the bottom layer were saturated with hydrogen atoms. Equilibrium atomic positions were determined by relaxation within a force convergence criterion of 50 meV/Å.

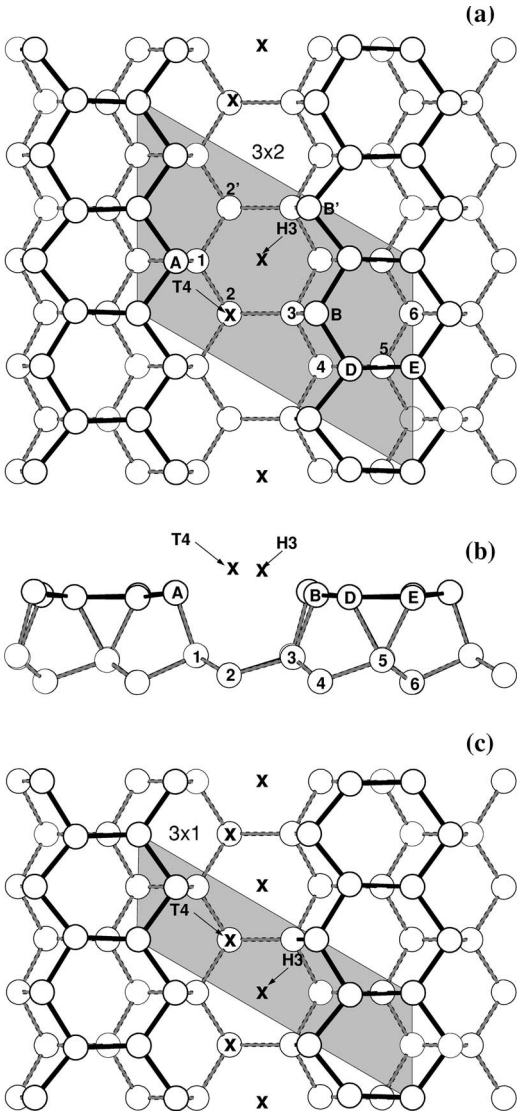

FIG. 1. Structural models for the Ca/Si(111)-(3×2) and -(3×1) surfaces. "×"s" indicate the possible *T*4 or *H*3 Ca adsorption sites. The surface unit cells are indicated by the shaded areas. (a) Top view of the (3×2) phase, (b) side view of the (3×2) phase, and (c) top view of the (3×1) phase.

III. RESULTS AND COMMENTS

Figure 1 presents the structural models of the (3×2) [Figs. 1(a) and 1(b)] and (3×1) [Fig. 1(c)] phases on Ca/Si(111). For both models the Ca adatoms are adsorbed on the *T*4 or *H*3 sites along the surface trench, separated by Si honeycomb chains. Comparing the Ca adsorption energies, we find that the *T*4 sites are energetically more favorable (compared with the *H*3 sites) by 0.02 eV/atom and 0.05 eV/atom for the (3×2) and (3×1) phases, respectively. These slight energy differences, favoring the *T*4 sites, are in accordance with the recent investigation performed by Lee *et al.*,[21] where the authors find that the *T*4 sites are energetically more favorable by 0.01 eV/atom for the Ba/Si(111)-(3×2) surface.

Having established that *T*4 corresponds to the energetically more stable adsorption sites for Ca adatoms on

TABLE I. Equilibrium geometry of the Ca/Si(111)-(3×2) surface, with the Ca adatoms on the *T*4 sites. The equilibrium distances are in Å.

	Ca-A	Ca-B	Ca-2	*B-D*	*D-E*	*E-A*	*A*-1	1-2	2-3	*B-B′*	2-2′
Bond length	3.03	2.96	3.63	2.36	2.30	2.36	2.40	2.38	2.40		
Vertical distance	0.62	0.70	3.62	0.07	0.05	0.09	2.28	0.72	0.66	0.12	0.01

Ca/Si(111), we next examined the relative energetic stability of the (3×2) and (3×2) surface phases. The energetic stability can be inferred by comparing the total energies of the Ca/Si(111)-(3×2) and -(3×1) surfaces, expressed as

$$\Delta E = E[(3\times 1)] - E[(3\times 2)] - \mu_{\mathrm{Ca}}.$$

Here $E[(3\times2)]$ and $E[(3\times1)]$ represent the total energies of Ca/Si(111)-(3×2) and -(3×1) surfaces, respectively. These total energies were obtained by using the same calculational procedure, including the same size of the supercell. As these two surfaces are not stoichiometrically equivalent with respect to the Ca concentration, we have to include the Ca chemical potential (μ_{Ca}), with the constraint that the maximum value of the Ca chemical potential correspond to the chemical potential of its bulk elemental phase—viz., $\mu_{\mathrm{Ca}} \leqslant \mu_{\mathrm{Ca}}^{\mathrm{bulk}}$. To assure the same convergence criterion, $\mu_{\mathrm{Ca}}^{\mathrm{bulk}}$ was also obtained by using the same calculation procedure as used for the surface calculations. Under the Ca-rich limit $\mu_{\mathrm{Ca}} \rightarrow \mu_{\mathrm{Ca}}^{\mathrm{bulk}}$, we find $\Delta E = 0.026$ eV/1×1. This indicates that even in the Ca-rich environment the (3×1) phase is not expected to occur on the Ca/Si(111) surface.

The formation of the (3×2) phase with a Ca coverage of 1/6 ML, instead of the (3×1) phase with a Ca coverage of 1/3 ML, is in good agreement with a recent experimental investigation performed by Sakamoto *et al.*[20] and Kim *et al.*[23] However, our findings are in contrast with the proposed (3×1) structural model (for a Ca coverage of 1/3 ML) obtained by photoemission experiments and *ab initio* calculations.[18] Further STM investigations[19] proposed a twofold periodicity along the honeycomb chains of the Ca/Si(111) surface, giving rise to a (3×"2") phase with a Ca coverage of 1/3 ML, where the two Ca adatoms of the 3×2 surface unit cell are "slightly shifted from *T*4 sites." We examined this proposed (3×"2") phase, and our total energy results indicated that the Ca-shifted configuration is not energetically stable. In fact the shifted Ca adatoms move symmetrically toward the *T*4 sites, thus becoming a (3×1) phase.

The equilibrium geometry of the (3×2) phase is summarized in Table I. For the topmost Si atoms we have used the same atomic labels as used in Ref. 20. The bond distances between the topmost Si atoms bonded to the Ca adatom, Ca-Si(*A*) and Ca-Si(*B*), are very similar, being slightly larger than the sum of the covalent radii of Ca and Si, 2.90 Å. The Si(*D*)-Si(*E*) bonds, along the honeycomb chain, are compressed by 0.06 Å compared with the Si-bulk equilibrium bond length (2.36 Å)). However, such a bond compression is not due to the Ca adsorption along the surface trench, since on the clean Si(111)-(3×2) surface the Si(*D*)-Si(*E*) bond length is equal to 2.29 Å. The Si(*B*) atoms bonded to the Ca adatoms are pushed downward by 0.12 Å with respect to the Si(*B′*) atoms (not bonded to the Ca adatoms). Meanwhile, the vertical positions of the second sublayer Si(2) atoms, lying just below the *T*4 sites, do not change due to the Ca adsorption process, indicating a weak interaction between Si(2) and the Ca adatom.

Figure 2 exhibits the structural model for the Ca/Si(111)-(2×1) surface with a Ca coverage of 0.5 ML. The (2×1) structural model was previously proposed in Refs. 18–20, with the Ca adatoms along the surface trench between two Si zigzag chains. Similar to the (3×2) model, we find that the Ca adsorption on *T*4 is energetically more favorable (by 0.03 eV/atom) compared with the Ca adsorption on *H*3. In Table II, we summarize our calculated equilibrium geometry for the Ca/Si(111)-(2×1) surface. The bond lengths between Ca adatoms and the topmost Si(*F*) and Si(*G*) atoms (3.00 and 3.02 Å, respectively) are almost the same. The vertical distance between the Ca adatoms and the second sublayer Si(2) atoms, lying just below the *T*4 sites, is 0.28 Å smaller compared with the vertical distance Ca-Si(2) in the (3×2) phase. In Ref. 20 the authors suggested that the atomic distances between the Ca adatoms and the topmost Si atoms for the (2×1) phase are larger compared with the Ca-Si bond lengths of the (3×2) phase. Indeed we

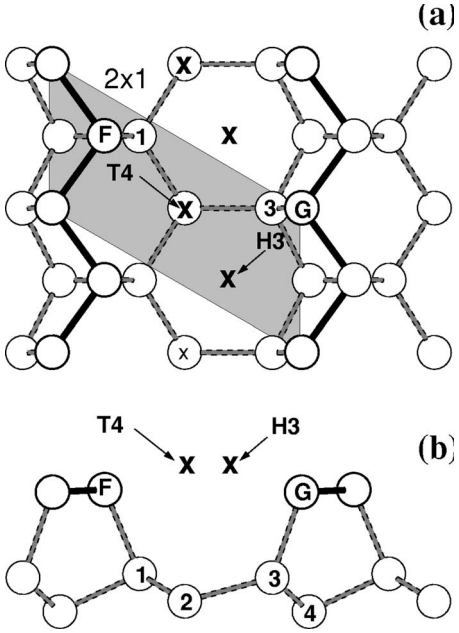

FIG. 2. Structural models for the Ca/Si(111)-(2×1) surface. The 2×1 surface unit cell is indicated by the shaded area, and "×"s" indicate the *T*4 or *H*3 Ca adsorption sites. (a) top view and (b) side view.

TABLE II. Equilibrium geometry of the Ca/Si(111)-(2×1) surface, with the Ca adatoms on the $T4$ sites. The equilibrium distances are in Å.

	Ca-F	Ca-G	Ca-2	*F*-*G*	*G*-1	1-2	2-3
Bond length	3.00	3.02	3.35	2.38	2.44	2.39	2.42
Vertical distance	0.36	0.43	3.34	0.07	2.25	0.74	0.63

find that the bond lengths between Ca adatoms and the Si atoms facing the adsorbate, Si(G) and Si(B), are larger for the (2×1) phase. However, the same does not occur for the Ca-Si(F) and Ca-Si(A) bonds. In this case, the Ca-Si bond length is slightly larger for the (3×2) surface.

Table III presents the electronic charge transfers on the Ca/Si(111)-(3×2) and -(2×1) surfaces based on a Mulliken population analysis. We find that the topmost Si atoms increase their charge densities compared with the charge density of the Si bulk, while the charge density of the Ca adatom is reduced by $0.72e$ and $0.64e$ for the (3×2) and (2×1) phases, respectively. The electronic charge transfer occurs from the Ca adatoms to the Si(111) surface, being smaller in the (2×1) surface phase, which is in accordance with the Si $2p$ core level investigations performed by Sakamoto *et al.*[20] They assigned to the topmost Si atoms (bonded to the Ca adatoms) two surface components named $S1$ and $S2$, with lower binding energies compared with the Si bulk component. From Table III, we find that (i) the charge densities of Si(A) and Si(F) are larger compared with the charge densities of Si(B) and Si(G), respectively, and (ii) the charge density difference between Si(A) and Si(B), $0.01e$, is smaller compared with the charge density difference between Si(F) and Si(G), $0.05e$. In agreement with Ref. 20, in (i) we can infer that the $S1$ component comes from Si(A) and Si(F) for the (3×2) and (2×1) phases, respectively. While from (ii) we can infer that the energy difference between the $S1$ and $S2$ components is smaller in the (3×2) surface, compared with the energy difference between $S1$ and $S2$ in the (2×1) phase. It is important to note that what we have, based upon charge transfer analysis, is a qualitative picture for the core-level energy shifts. Meanwhile, a quantitative analysis can be obtained by considering the "initial-state" and the "final-state" electron-core relaxation processes, as decribed in Refs. 32 and 33.

A third surface component ($S3$) was observed for higher binding energies compared with the Si-bulk component. The authors attributed such $S3$ component to the second sublayer Si atoms below the $T4$ sites adsorbed by Ca adatoms [Si(2) in Figs. 1 and 2]. For the (3×2) structure we find that the charge density of Si(2) decreases, suggesting an increase of the binding energy compared with the Si bulk component. In contrast, in the (2×1) model the charge density of Si(2) increases, thus indicating a reduction of the binding energy. Moreover, they find that the energy position of $S3$ is the same for both structural models. Those results suggest that the $S3$ component cannot be due to the Si(2) atoms. On the other hand, we find that the subsurface Si atoms, just below the topmost honeycomb chains or below the zigzag chains [Si(5) in Fig. 1 and Si(4) in Fig. 2], decrease their charge density by almost the same amount, $0.11e-0.12e$. Therefore, we propose that the $S3$ component comes from the subsurface Si(5) and Si(4) atoms in the (3×2) and (2×1) phases, respectively. We believe that further experimental investigations are necessary to clarify the origin of the S3 component.

Figures 3(a) and 4(a) exhibit the total charge densities along the honeycomb chains and zigzag chains of the (3×2) and (2×1) surfaces, respectively. For both structural models, we verify the formation of covalent bonds along the Si chains. In order to localize the electronic states near the fundamental band gap of the Ca/Si(111) surface, we calculated the higher-lying (lower-lying) occupied (empty) electronic states projected onto a (111) plane at 1.25 Å above the Ca adatoms. Within the Tersoff-Hamann approach,[34] our calculated projected local density of states, depicted in Figs. 3(b), 3(c), 4(b), and 4(c), correspond to the STM images of the Ca/Si(111) surfaces.[35,36] In Fig. 3(b) we present the electronic distribution of higher-lying occupied electronic states, within an energy range of 2 eV below the calculated Fermi energy. We find that the highest occupied states are localized on the topmost Si atoms: Si(A), Si(B), and Si(B'). In the same diagram, we identify a (electronic) pairing effect among the Si(A) atoms, giving rise to the $\times2$ periodicity along the honeycomb chain. The formation of a trimerlike configuration as well as the $2\times$ pairing effects is ruled by electrostatic attractive interactions between the Ca adatoms and the nearest-neighbor Si atoms. Similar $\times2$ modulation was observed for the Ba/Si(111)-(3×2) surface.[21] In Fig. 3(c) we present the lower-lying empty states within an en-

TABLE III. Electronic charge transfers, based on Mulliken analysis, for Ca/Si(111)-(3×2) and Ca/Si(111)-(2×1) surfaces. The indicated values are in electrons/atom.

(3×2)	Ca	*A*	*B*	*D*	*E*	2′	2	5
Charge transfer	−0.72	0.33	0.32	0.07	0.06	0.06	−0.05	−0.12
2×1	Ca	*F*	*G*				2	4
Charge transfer	−0.64	0.32	0.27				0.02	−0.11

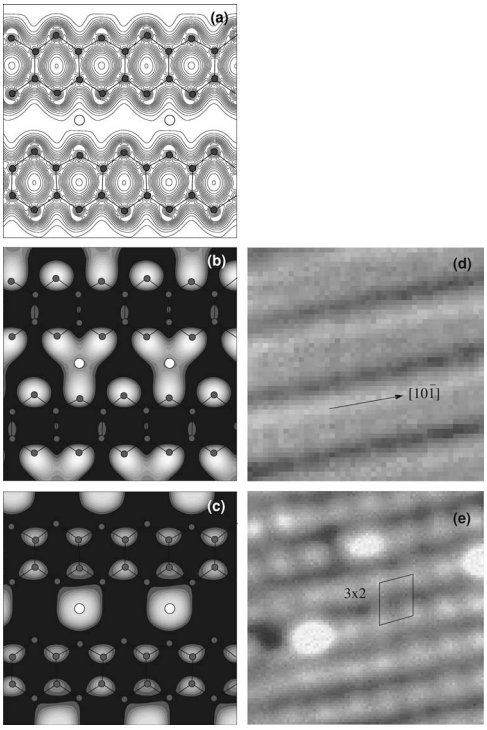

FIG. 3. (a) Top view of the total charge density of the Ca/Si(111)-(3×2) surface. (b) Simulated STM images of occupied states within an energy range 2 eV below the calculated Fermi energy. Simulated STM images of empty states within an energy range of (c) 2 eV above the Fermi energy. Experimentally obtained STM image for (d) occupied and (e) unoccupied states (bias voltage of 1.8 V) from Ref. 19.

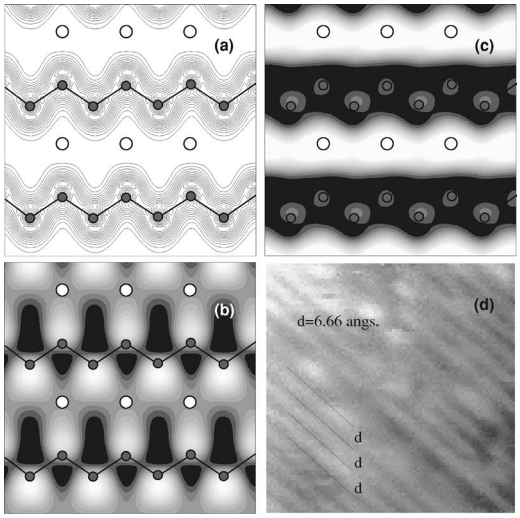

FIG. 4. (a) Top view of the total charge density for the Ca/Si(111)-(2×1) surface. (b) Simulated STM images of occupied states within an energy range of 2 eV below the calculated Fermi energy. (c) Simulated STM images of empty states within an energy range of 2 eV above the calculated Fermi energy. (d) Experimentally obtained STM images, for unoccupied states (bias voltage of 1.8 V) from Ref. 19.

ergy interval of 2 eV above the calculated Fermi energy, where we verify that the empty states are mainly concentrated on the Ca adatoms. In this case we find that the bright protrusions, concentrated on the Ca adatoms, exhibit a 3×2 surface periodicity with one bright spot for each (3×2) surface unit cell. In Figs. 3(d) and 3(e) we present experimental STM images for filled and empty states, respectively, obtained by Sekigushi *et al.*[19] For filled states they verify the formation on double and asymmetric bright rows parallel to the honeycomb chains (i.e., [10$\bar{1}$] direction) with different periodicities 2× and 1× along the [10$\bar{1}$] direction. Meanwhile for empty states, they find bright spots with 3×2 periodicity, in agreement with previous STM pictures for the Ca/Si(111) surface obtained by Saranin *et al.*[15,16] Similar STM images (for empty states) were also obtained for another AEM on Si(111), Mg/Si(001)-(3×2).[14] Those experimental STM findings are in good agreement with our calculated results—viz., (i) formation of two parallel and asymmetric bright lines with ×2 and ×1 modulations lying along the Si honeycomb chains [Figs. 3(b) and 3(d)] for filled states and (ii) formation of one bright spot with (3×2) surface periodicity lying on the Ca adatom [Figs. 3(c) and 3(e)], for empty states.

For the Ca/Si(2×1) surface, within an energy range of 2 eV below the calculated Fermi energy [cf. Fig. 4(b)], the occupied electronic states are localized on the Si(*F*) and Si(*G*) atoms, being slightly more concentrated on the Si(*F*) atoms with no contribution from the Ca adatoms. Meanwhile, the empty states within an energy interval of 2 eV above the Fermi energy, depicted in Fig. 4(c), are concentrated on the Ca adatoms forming bright stripes parallel to the Si zigzag chains, [10$\bar{1}$] direction. Figure 4(d) exhibits the experimentally obtained STM image (empty states) obtained in Ref. 19. The bright stripes are aligned along the [10$\bar{1}$] direction, being separated by d=6.66 Å, which is in nice agreement with our simulated STM image for empty states, Fig. 4(c). We find that the bright stripes lie on Ca adatoms, with lateral distance of 6.65 Å between two consecutive lines. Comparing our simulated STM images, for the (3×2) and (2×1) models, we can infer that the occupied states within an energy interval of ~2 eV near to the Fermi level are localized on the topmost Si atoms of the honeycomb and zigzag chains for the (3×2) and (2×1) Ca/Si(111) surfaces, respectively. The empty states near to the Fermi energy (within the same energy range, ~2 eV) lie on the Ca adatoms; however, the electronic distributions of these states are very different. For the Ca/Si(111)-(3×2) surface, the empty states are localized on the Ca adatoms, with no wave function overlap parallel to the [10$\bar{1}$] direction. Meanwhile, there is a strong wave function overlap, for the empty states, parallel to the [10$\bar{1}$] direction for the Ca/Si(111)-(2×1) surface.

In order to improve our understanding of the electronic properties of Ca lines on Si(111) and support the recent experimental findings,[22,23] we calculate the electronic band structure around the fundamental energy gap region for Ca/Si(111)-(3×2) [Fig. 5(a)] and Ca/Si(111)-(2×1) [Fig. 5(b)] surfaces. The shaded areas represent the projected Si bulk band structure, and the Γ-$\bar{J}$ (Γ-$\bar{J}'$) direction is parallel

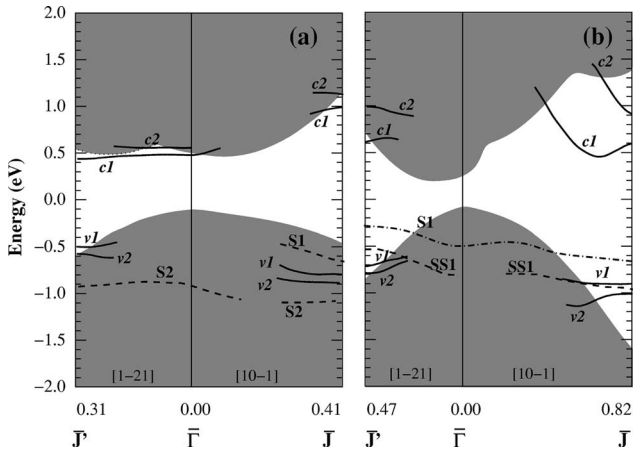

FIG. 5. Electronic band structure along the $\bar{\Gamma}$-$\bar{J}'$ and $\bar{\Gamma}$-$\bar{J}$ directions. In (a), for the Ca/Si(111)-(3×2) surface, the $\bar{\Gamma}$-$\bar{J}'$ ($\bar{\Gamma}$-$\bar{J}$) direction is perpendicular (parallel) to the honeycomb chains. In (b) for the Ca/Si(111)-(2×1) surface, the $\bar{\Gamma}$-$\bar{J}'$ ($\bar{\Gamma}$-$\bar{J}$) direction is perpendicular (parallel) to the Si zigzag chains. In both diagrams we present the experimental data points of Refs. 22 (dot-dashed lines) and 23 (dashed lines). The $k_{\|}$ wave vectors are in Å^{-1}.

(perpendicular) to the Ca lines. The states labeled vi ($i=1$ and 2) are occupied surface states, while the states labeled ci ($i=1$ and 2) are unoccupied surface states. The experimental results are indicated by dot-dashed[22] and dashed[23] lines, while our calculated results are indicated by solid lines. Both structural models (3×2) and (2×1) are semiconducting, with the occupied states lying below the Si-bulk valence-band maximum (VBM). For the (3×2) model, along the Γ-$\bar{J}$ direction we find two electronic states $v1$ and $v2$, resonant within the Si bulk projected band structure. The main contributions to $v1$ and $v2$ states come from $3p_y$ and $3p_z$ orbitals of the Si adatoms along the edge of the honeycomb chain, Si(A), Si(B), and Si(B'), being slightly more concentrated on Si(B'). We find binding energies around 0.7 eV ($v1$) and 0.8 eV ($v2$) below the VBM for $k_{\|}=0.41$ Å^{-1}. The $v1$ state compares very well with the experimentally obtained $S1$ state (dashed line). $S1$ lies at $\sim$0.55 eV below the VBM, being also resonant within the projected valence band with downward dispersion along the Γ-$\bar{J}$ direction. For wave vectors parallel to the Γ-$\bar{J}'$ direction (perpendicular to the Ca lines), with $k_{\|}=0.31$ Å^{-1}, we find $v1$ and $v2$ with binding energies of $\sim$0.4 and $\sim$0.5 eV below the VBM. We believe that these states cannot be compared with $S2$ (binding energy of 0.8 eV below the VBM). However, in Ref. 23 the authors verified an occupied state ($S1$) near to the edge of the projected valence band for $k_{\|}\approx0.35$ Å^{-1} (not shown), which can be compared with $v1$ and $v2$. Along the Γ-$\bar{J}'$ direction the $c1$ state lies slightly below the conduction-band minimum (CBM) with flat energy dispersion. Similar almost flat energy dispersion was verified for $c1$ and $c2$ along the Γ-$\bar{J}$ direction, parallel to the Ca lines. It is worth to pointing out that the energy dispersions of $c1$ and $c2$ are in agreement with the localized character of the STM images (for empty states) shown in Figs. 3(c) and 3(e).

Our calculated binding energies of $v1$, for the (2×1) surface [Fig. 5(b)], compare very well with the experimental results for wave vectors parallel to the Γ-$\bar{J}$ direction. We find a binding energy of 0.8 eV below the VBM for $k_{\|}=0.81$ Å^{-1}. This $v1$ state comes mainly from $3p_x$ orbital of the Si atoms along the zigzag chains, Si(F) and Si(G). The experimental results, dot-dashed (dashed) lines, indicate a binding energy of 0.6 eV (0.8 eV) below VBM for $k_{\|}=0.81$ Å^{-1}. In addition, we verify that the energy dispersion of $v1$ and the experimentally obtained $SS1$ and $S1$ surface states are in very good agreement. Along the Γ-$\bar{J}'$ direction we find two surface states near to $k_{\|}=0.47$ Å^{-1}, with binding energies of 0.6 eV ($v1$) and 0.8 eV ($v2$). $v1$ can be compared with $SS1$, a binding energy of 0.46 eV below VBM. However, our calculated energy dispersions along the $\Gamma\rightarrow\bar{J}'$ do not agree with the experimental measurements. For empty states $c1$ and $c2$, we find (large) energy dispersion along the Γ-$\bar{J}$ direction, in agreement with the formation of bright stripes parallel to the Ca lines for the Ca/Si(111)-(2×1) surface, Figs. 4(c) and 4(d).

IV. CONCLUSIONS

In summary, we have performed an *ab initio* theoretical investigation of the Ca/Si(111) surface, considering the (3×1), (3×2), and (2×1) structural models. Our total energy results indicate that the adsorption of Ca adatoms on the $T4$ sites, along the surface trench, is energetically more favorable compared with the $H3$ sites. Comparing the total energies of the (3×1) and (3×2) phases, we find that the (3×1) phase (with a Ca coverage of 1/3 ML) is not expected to occur even under Ca-rich conditions. The energetic stability of the (3×2) phase, for a Ca coverage of 1/6 ML, is in agreement with its semiconducting character inferred by simple electron counting analysis. In the equilibrium geometry, the Ca-Si bond distances for (3×2) and (2×1) phases are almost the same, $\sim$3 Å, being slightly larger than the sum of the covalent radii. Based upon a Mulliken population analysis we mapped the electronic charge transfers on the Ca/Si(111)-(3×2) and -(2×1) surfaces. We find that the amount of charge transfers from Ca adatoms toward the topmost Si atoms is larger in the (3×2) phase. In addition, we obtained a qualitative picture for the core level photoemission results of Ref. 20. Our simulated STM images indicate that the highest occupied states lie on the Si atoms at the edge of the honeycomb chains for the (3×2) phase and along the topmost Si zigzag-chains in the (2×1) model. The formation of trimerlike structure, for the occupied states of the (3×2) phase, confirms the experimentally observed $2\times$ and $1\times$ modulations parallel to the Ca lines. The simulated STM picture for empty states indicates the formation of bright spots and lines on the Ca adatoms for the (3×2) and (2×1) phases, in good agreement with the experimentally

obtained STM images. Our electronic band structure calculations confirm the semiconducting character of the Ca/Si(111)-(3×2) and -(2×1) surfaces. Comparing our calculated results with the recent experimental ARPES measurements, we provide additional support to the proposed structural models for the Ca/Si(111) surface.

ACKNOWLEDGMENTS

The author acknowledges Professor G. P. Srivastava and Professor P. Venezuela for their comments and suggestions on the manuscript. This work received financial support from the Brazilian agencies CNPq and FAPEMIG.

[1] H. W. Yeom *et al.*, Phys. Rev. Lett. **82**, 4898 (1999).
[2] I. G. Hill and A. B. McLean, Phys. Rev. Lett. **82**, 2155 (1999).
[3] K. Miki, D. R. Bowler, J. H. G. Owen, G. A. D. Briggs, and K. Sakamoto, Phys. Rev. B **59**, 14868 (1999).
[4] M. Naitoh, H. Shimiya, S. Nishigaki, N. Oishi, and F. Shoji, Appl. Surf. Sci. **142**, 38 (1999).
[5] M. Naitoh, M. Takei, S. Nishigaki, N. Oishi, and F. Shoji, Surf. Sci. **482-485**, 1440 (2001).
[6] J. H. G. Owen, D. R. Bowler, and K. Miki, Surf. Sci. Lett. **499**, L124 (2002).
[7] J. H. G. Owen, K. Miki, and D. R. Bowler, Surf. Sci. Lett. **527**, L177 (2003).
[8] R. H. Miwa and G. P. Srivastava, Surf. Sci. **473**, 123 (2001).
[9] R. H. Miwa, T. M. Schmidt, and G. P. Srivastava, Surf. Sci. **507-510**, 368 (2002).
[10] J. H. G. Owen, K. Miki, H. Koh, H. W. Yeom, and D. R. Bowler, Phys. Rev. Lett. **88**, 226104 (2002).
[11] R. H. Miwa and G. P. Srivastava, Phys. Rev. B **66**, 235317 (2002).
[12] S. C. Erwin and H. H. Weitering, Phys. Rev. Lett. **81**, 2296 (1998).
[13] K. An, R. Park, J. Kum, C. Park, C. Kim, J. Chung, T. Abukawa, S. Kono, T. Kinoshita, and T. Ishii, Surf. Sci. Lett. **337**, L789 (1995).
[14] O. Kubo, A. A. Saranin, A. V. Zotov, J.-T. Ryu, H. Tani, T. Harada, M. Katayama, V. Lifshits, and K. Oura, Surf. Sci. Lett. **415**, L971 (1998).
[15] A. A. Saranin, A. Zotov, V. G. Lifshits, M. Katayama, and K. Oura, Surf. Sci. **426**, 298 (1999).
[16] A. A. Saranin, V. G. Lifshits, K. I. Ignatovich, H. Bethge, R. Kayser, H. Goldbach, A. Klust, J. Wollschläger, and M. Henzler, Surf. Sci. **448**, 87 (2000).
[17] M. A. Olmstead, R. I. G. Uhrberg, R. D. Bringans, and R. Z. Bachrach, J. Vac. Sci. Technol. B **4**, 1123 (1986).
[18] A. A. Baski, S. C. Erwin, M. S. Turner, K. M. Jones, J. W. Dickinson, and J. A. Carlisle, Surf. Sci. **476**, 22 (2001).
[19] T. Sekigushi, F. Shimokoshi, T. Nagao, and S. Hasegawa, Surf. Sci. **493**, 148 (2001).
[20] K. Sakamoto, W. Takeyama, H. M. Zhang, and R. I. G. Uhrberg, Phys. Rev. B **66**, 165319 (2002).
[21] G. Lee, S. Hong, H. Kim, D. Shin, J.-Y. Koo, H.-I. Lee, and Dae Won Moon, Phys. Rev. Lett. **87**, 056104 (2001).
[22] K. Sakamoto, H. M. Zhang, and R. I. G. Uhrberg, Phys. Rev. B **68**, 245316 (2003).
[23] Y. K. Kim, J. W. Kim, H. S. Lee, Y. J. Kim, and H. W. Yeom, Phys. Rev. B **68**, 245312 (2003).
[24] P. Hohenberg and W. Kohn, Phys. Rev. **136**, B864 (1964).
[25] J. M. Soler, E. Artacho, J. D. Gale, A. García, J. Junquera, P. Ordejón, and D. Sánchez-Portal, J. Phys.: Condens. Matter **14**, 2745 (2002).
[26] W. Kohn and L. J. Sham, Phys. Rev. **140**, A1133 (1965).
[27] O. F. Sankey and D. J. Niklewski, Phys. Rev. B **40**, 3979 (1989).
[28] E. Artacho, D. Sánchez-Portal, P. Ordejón, A. Garcia, and J. M. Soler, Phys. Status Solidi B **215**, 809 (1999).
[29] D. M. Ceperley and B. J. Alder, Phys. Rev. Lett. **45**, 566 (1980).
[30] J. P. Perdew and A. Zunger, Phys. Rev. B **23**, 5048 (1981).
[31] L. Kleinman and D. M. Bylander, Phys. Rev. Lett. **48**, 1425 (1982).
[32] E. Pehlke and M. Scheffler, Phys. Rev. Lett. **71**, 2338 (1993).
[33] A. Pasquarello, M. S. Hybertsen, and R. Car, Phys. Rev. B **53**, 10942 (1996).
[34] J. Tersoff and D. R. Hamann, Phys. Rev. B **31**, 805 (1985).
[35] G. Brocks, P. J. Kelly, and R. Car, Phys. Rev. Lett. **70**, 2786 (1993).
[36] R. H. Miwa and G. P. Srivastava, Phys. Rev. B **63**, 125341 (2001).